Check for updates

A carbon membrane-mediated CdSe and TiO$_2$ nanofiber film for enhanced photoelectrochemical degradation of methylene blue†

Xinye Zhang,[a] Xueyue Zhang,[a] Keting Feng,[a] Xiaoyun Hu, [ID][b] Jun Fan [ID][a] and Enzhou Liu [ID]*[a]

In this study, a carbon membrane-mediated CdSe and TiO$_2$ ternary film (CdSe/C/TiO$_2$) was prepared to degrade methylene blue (MB). Carbon membrane and CdSe were introduced to the surface of a TiO$_2$ nanofiber film *via* an *in situ* hydrothermal deposition process successively. The investigation shows that the carbon membrane not only provides a charge transfer channel to promote the transfer of electron from the conduction band of CdSe to that of TiO$_2$, but also improves the poor conduct between the TiO$_2$ film and electrolyte. The synergies between the carbon membrane and CdSe can make the ternary system harvest more visible light energy and facilitate the charge transfer property of TiO$_2$. The current density of CdSe/C/TiO$_2$ was about 9 folds higher compared with that of pure TiO$_2$ under UV and visible light irradiations. This ternary hybrid exhibits a superior activity during the photoelectrochemical (PEC) degradation of MB, and 92.43% can be removed after 120 min irradiation, which is improved by 21.14% than that of TiO$_2$.

1. Introduction

Waste discharge from chemical industries is threatening to the health of human beings.[1] The waste-related environmental problems need to be solved urgently.[2,3] In the past few years, numerous traditional ways have been employed in disposing water pollution including absorption, photocatalysis, electrocatalysis, and microbiological degradation.[4–8] However, the above-mentioned solutions suffer from high cost, low efficiency, secondary pollution, and so on.[9–11] At present, compared with photocatalysis and electrocatalysis, photoelectrocatalytic degradation has received considerable attention owing to its low cost, sustainability and high efficiency, which can decompose the organic pollutants into H$_2$O and CO$_2$ completely.[12–17] Until now, numerous photoelectrocatalysts have been developed for the photoelectrochemical (PEC) processes, such as TiO$_2$, ZnO, and MnO$_2$.[18–20] Among them, TiO$_2$ has been widely investigated for its physical and chemical stability, non-toxicity and available properties.[21,22]

However, there are still limitations for the practical applications of TiO$_2$: (1) its inherent band gap of 3.0–3.2 eV leads to poor visible light capture ability; (2) fast recombination of the charge carriers results in an inefficient photoexcitation process;

(3) the powder form of TiO$_2$ makes it hard to reuse for the separation problems.[23,24] In the last few decades, various strategies have been employed to improve the activity of TiO$_2$. For example, metal doping (Au, Ag, Pt, Ni, *etc.*),[25–28] coupling with narrow-gap semiconductors (ZnSe, CdSe, CdS, *etc.*),[29–33] and introducing carbon-based materials.[34]

Investigations demonstrate that the combination of TiO$_2$ with narrow band gap semiconductors to form heterojunctions is an effective strategy to achieve wider range of light absorption and faster separation of charge carrier simultaneously.[35–37] Recently, CdSe with a suitable conduction band position and an ideal band gap (1.7 eV) has been widely used for the sensitization of TiO$_2$. The hybrids can be applied in H$_2$ evolution, CO$_2$ reduction and pollutants degradation.[38–41] Xu *et al.* used CdSe/TiO$_2$ powder to degrade MB, and the removal efficiency was 90.5% after 5 h of irradiation.[42] Although the above-mentioned heterojunction can promote charge transfer and improve the light harvesting ability of TiO$_2$, the question that remains is CdSe, a small-diameter-particle, randomly combined with TiO$_2$ cannot solve the problem of poor contact between the TiO$_2$ photoanode and the electrolyte, which is proved to be the key point in improving the PEC efficiency.

Carbon materials (graphene, carbon quantum dots, carbon nanofibers, carbon membrane, *etc.*) have been widely employed to improve the PEC activity of TiO$_2$.[43–47] They not only provide a carrier transport channel to accelerate the carrier transfer but also promote the contact properties between TiO$_2$ and electrolyte.[48–50] Gao *et al.* used γ-graphene to enhance the activity of TiO$_2$ nanotube arrays, and the degradation rate of rhodamine B

[a]School of Chemical Engineering, Xi'an Key Laboratory of Special Energy Materials, Northwest University, Xi'an, 710069, P. R. China. E-mail: ok.208@163.com

[b]School of Physics, Northwest University, Xi'an, 710069, P. R. China

† Electronic supplementary information (ESI) available. See DOI: 10.1039/d1ra01240a

was increased slightly (1.35 times).[51] Liu *et al.* used carbon quantum dots to facilitate the charge transfer between $Cd_{0.5}Zn_{0.5}S$ and TiO_2 nanorod film (CZS/C/TiO₂ NRF), the photocurrent density was boosted to 8.19 μA cm⁻².[52] It is confirmed that carbon materials can greatly improve the PEC activity of TiO_2 with excellent PEC performance. However, graphene and carbon nanofibers are difficult to prepare, and carbon quantum dot is hard to separate during the preparation and it easily falls off from the substrate. Recently, Zhang *et al.* used a simple strategy to introduce a carbon membrane on TiO_2 nanotube arrays, and this nanofilm can be easily separated and reused for its excellent stability.[53] Even so, there are few researches on the use of carbon membranes in PEC degradation.

In this study, a carbon membrane-bridged CdSe and TiO_2 ternary film (CdSe/C/TiO₂) was prepared *via* an *in situ* hydrothermal deposition process successively. We found that the carbon membrane, as a carrier-transfer-channel, can accelerate the electron migration from the conduction band of CdSe to that of TiO_2, and improve the poor contact between TiO_2 and electrolyte. The current density of CdSe/C/TiO₂ (45.36 μA cm⁻²) was about 9 times compared with that of pure TiO_2 (5.42 μA cm⁻²) under UV and visible light irradiations, and the performance of the ternary CdSe/C/TiO₂ film was tested in the photoelectrocatalytic degradation of MB. The results reveal that the degradation efficiency of CdSe/C/TiO₂ (92.43%) significantly increased by 21.14% than that of the pure TiO_2. Finally, the PEC mechanism over the CdSe/C/TiO₂ nanofiber film was proposed based on the PEC analyses and free radical capture experiments.

2. Experimental processes

2.1 Preparation of the CdSe/C/TiO₂ nanofiber film

A TiO_2 nanofiber film was obtained *via* a hydrothermal process, followed by acidification and annealing treatments. As shown in Scheme 1, a Ti sheet (20 × 40 × 0.2 mm) was first chemically polished using a mixed acid solution consisting of HF, HNO₃ and H₂O to remove surface impurities. Subsequently, 2 g NaOH was dissolved in 25 mL of ethylene glycol and 25 mL of deionized water, and stirred for 30 min. Then, the polished Ti sheet was put into a Teflon-lined stainless steel vessel with the above solution together, sealed and heated at 180 °C for 24 h. Hereafter, the sample was acidified in HCl (0.25% wt) for 24 h.

Finally, the TiO_2 nanofiber film was obtained after calcination at 350 °C for 2 h at a heating rate of 5 °C min⁻¹.

A carbon membrane was coated on the TiO_2 nanofilm *via* a simple hydrothermal process. 0.432 g glucose and 0.042 g ascorbic acid were added into 50 mL of H₂O under stirring. Subsequently, the TiO_2 nanofiber film and above mixture were sealed in a Teflon-lined stainless steel vessel, and heated at 80 °C for 12 h to obtain the C/TiO₂ nanofiber film.

The CdSe/C/TiO₂ ternary film was prepared *via* a hydrothermal process too. 0.0237 g Se powder was dissolved in 40 mL of diethylenetriamine (solution A), and then CdCl₂ was dissolved in 10 mL of H₂O (solution B). Subsequently, solution A and solution B were mixed under stirring and then transferred into a Teflon-lined stainless steel vessel. Further, the above C/TiO₂ nanofiber film was immersed into this mixture, sealed and maintained at 160 °C for 12 h. After cooling naturally, the film was washed using deionized water and ethanol, and dried at room temperature to obtain the CdSe/C/TiO₂ ternary nanofiber film.

2.2 Characterization

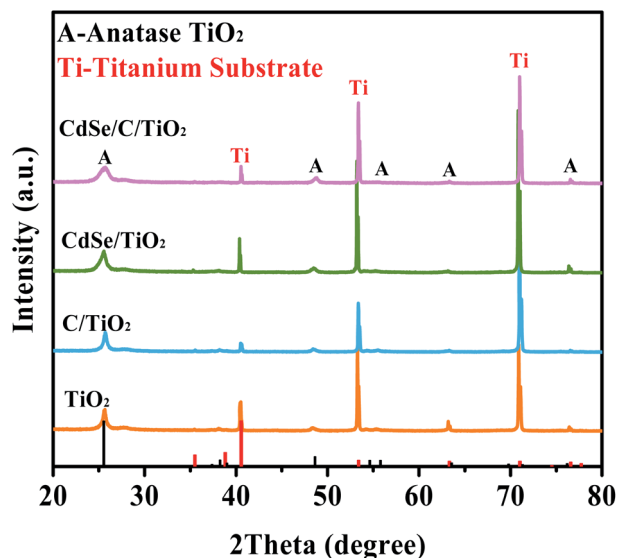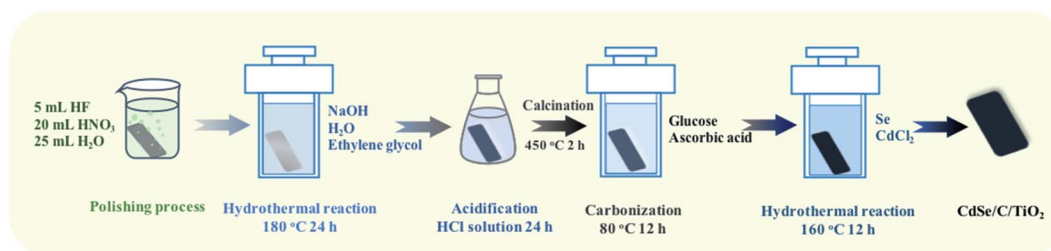The ESI† provide details of characterization, PEC measurements and PEC performance test.

Fig. 1 XRD patterns of the samples.

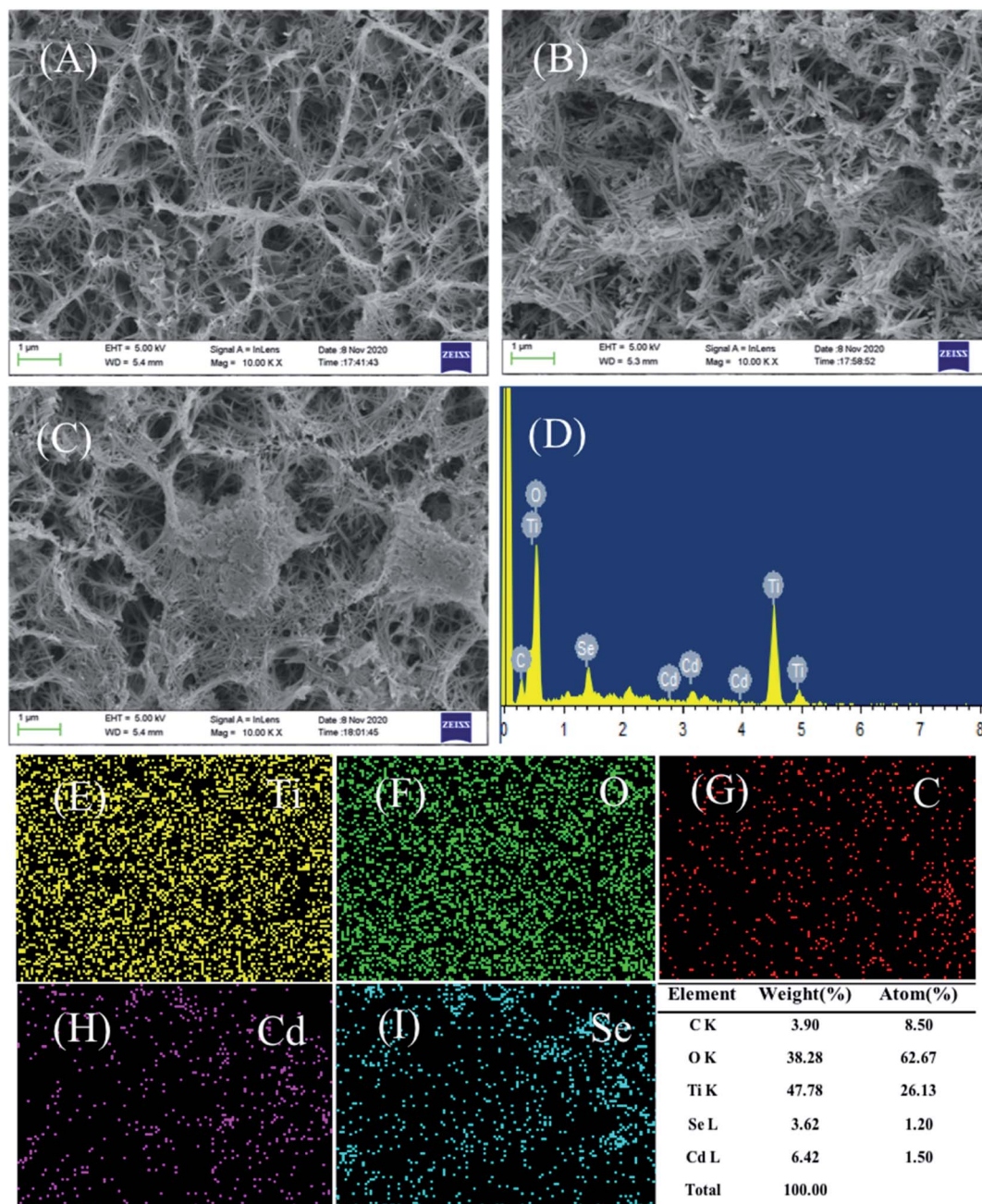**Scheme 1** Preparation processes of the CdSe/C/TiO₂ nanofiber film.

Element	Weight(%)	Atom(%)
C K	3.90	8.50
O K	38.28	62.67
Ti K	47.78	26.13
Se L	3.62	1.20
Cd L	6.42	1.50
Total	**100.00**	

Fig. 2 (A–C) SEM images of all samples: (A) pure TiO_2, (B) C/TiO_2, and (C) $CdSe/C/TiO_2$; (D) EDS of $CdSe/C/TiO_2$; (E–I) elemental mapping images for Ti, O, C, Cd and Se.

3.   Results and discussion

Fig. 1 presents the X-ray diffraction (XRD) patterns of the sample. The characteristic diffraction peaks of anatase TiO_2 are observed in all the samples. Peaks at $25.69°$, $48.79°$, $54.77°$, $55.94°$, $63.14°$ and $76.37°$ belong to the crystal surfaces of (101), (200), (105), (211), (213) and (215) of anatase TiO_2, respectively (JCPDS no. 75-1537).[54] Moreover, the peaks located at $40.17°$, $53.00°$ and $70.66°$ are assigned to the Ti sheet substrate (JCPDS no. 44-1294). Besides, the signals of the carbon membrane and CdSe are not observed due to the low content and poor

crystallinity of CdSe and the amorphous nature of carbon, but they can be observed by EDS and XPS.[46,54]

As shown in Fig. 2A–C, the TiO_2 film is composed of a large number of nanofibers intertwined to form a stable structure (nanofiber film), which is conducive to the light scattering and harvesting abilities of the TiO_2 film. This network structure becomes rougher when the carbon membrane is loaded (Fig. 2B). As shown in Fig. 2C, the CdSe nanoparticles are obviously supported on the C/TiO_2. Notably, the film-shape is easier for cyclic utilization than the powder form of TiO_2, which is beneficial for the practical application. According to the EDS
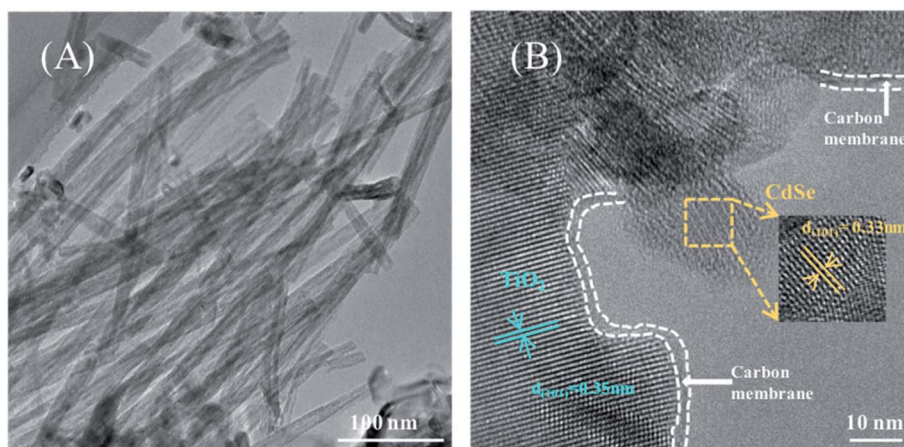
Fig. 3 (A) TEM and (B) HRTEM images of the CdSe/C/TiO$_2$ nanofiber film.

(Fig. 2D) and elemental mapping (Fig. 2E–I), it is obvious that there are signals of Ti, O, C, Cd and Se. It is confirmed that the carbon membrane and CdSe co-exist on the surface of the TiO$_2$ film with good dispersion.

The microstructure of the CdSe/C/TiO$_2$ nanofiber film is also investigated by TEM. As shown in Fig. 3A, nanofibers of TiO$_2$ with a reticular structure can be clearly observed, and it is well preserved after the deposition of the carbon membrane and CdSe. The HRTEM image in Fig. 3B clearly reveals that the inter-planar spacing of the crystal lattice is 0.35 nm, which is consistent with the (101) plane of anatase TiO$_2$. Besides, the carbon membrane is loaded on the surface TiO$_2$, and the thickness of the carbon membrane is about 2–3 nm. It is clearly seen that the CdSe particles are supported outside the carbon membrane, and the spacing of 0.35 nm belongs to the (101) plane of CdSe. Above TEM analysis further confirms the co-existence of carbon and CdSe on the surface of the TiO$_2$ nanofilm.

X-ray photoelectron spectroscopy (XPS) is an important technique to confirm the elements and their states over the surface of the materials.[55] As shown in the survey spectrum (Fig. 4A), the signals of Ti, O, C, Cd and Se can be detected. The corresponding high resolution spectra are shown in Fig. 4B–F. The spectrum of C 1s can be fitted into three peaks at 284.6, 286.1 and 288.1 eV in Fig. 4B, and they are attributed to the C–C, C–O and C=O, respectively.[56] As shown in Fig. 4C, the peaks at 458.3 and 464.0 eV correspond to Ti 2p$_{3/2}$ and Ti 2p$_{1/2}$, respectively.[57] The three peaks at around 529.6, 530.1 and 530.7 eV are ascribed to Ti–O, C=O and C–OH in the spectrum of O 1s (Fig. 4D), respectively, revealing the presence of carbon in this composite.[58] Moreover, the double peaks at 404.6 and 411.3 eV in Fig. 4E are designated to 3d$_{5/2}$ and 3d$_{3/2}$ of Cd^{2+}.[59] The peak at 50.7 eV in Fig. 4F indicates the existence of Se^{2-}.[60] Above proofs further confirm that the carbon membrane and CdSe co-exist on the surface of the TiO$_2$ nanofiber film.

Fig. 5A shows the UV-Vis absorption properties of the samples. All the samples exhibit absorption at the edge of 386 nm, corresponding to a band gap energy of 3.2 eV, which results from the inherent absorption of anatase TiO$_2$.[38] This interlacing network structure of TiO$_2$ leads to the irregular scattering effects of incident light, enhancing the light harvesting ability (Fig. 2A). After introducing CdSe particles, the absorption of CdSe/TiO$_2$ in the visible light range clearly got enhanced owing to the narrower band gap of CdSe. Carbon membrane can also capture visible light and further enhance the absorption capacity of the samples because of its unique optical properties.[61] These results indicate that the combination of carbon membrane and CdSe endows the ternary composite (CdSe/C/TiO$_2$) with excellent visible light absorption ability.

The photoluminescence (PL) spectra were obtained to illustrate the charge recombination efficiency, as shown in Fig. 5B. Under excitation at 220 nm, they all share same emission shapes around 400 and 465 nm. The emission intensity of C/TiO$_2$ and CdSe/TiO$_2$ are lower than that of the TiO$_2$ nanofiber film. After introducing the carbon membrane and CdSe, the PL emission intensity of CdSe/C/TiO$_2$ obviously decreased, suggesting that the recombination of electrons and holes is inhibited in this CdSe/C/TiO$_2$ heterojunction.

Fig. 6A presents the photocurrent density of the samples. The photocurrent density elevates quickly after the light illumination, and then decreases rapidly to 0 μA cm^{-2} under dark conditions, indicating that all the electrodes have very sensitive optical response. C/TiO$_2$ (29.52 μA cm^{-2}) and CdSe/TiO$_2$ (16.16 μA cm^{-2}) both exhibit higher photocurrent density than TiO$_2$ (5.42 μA cm^{-2}). In addition, the current density of the CdSe/C/TiO$_2$ film is 45.36 μA cm^{-2}, which is 9 folds enhancement compared to that of TiO$_2$, which indicates that more electrons can be effectively transferred from the CdSe/C/TiO$_2$ photoanode to the Pt counter electrode, which accelerates the separation of electrons and holes.

As displayed in Fig. 6B, open-circuit potential (V_{oc}) is used to further reveal its photoelectric property. When the Xe lamp is switched on, the photoelectrodes produce high photovoltages with better photosensitivity and stability, which benefits from the balance of accumulation and recombination of the charge carriers on the surface of the catalyst. Compared with pure TiO$_2$, all the samples exhibit higher electric potential than TiO$_2$. Among them, the ternary composite CdSe/C/TiO$_2$ exhibits the
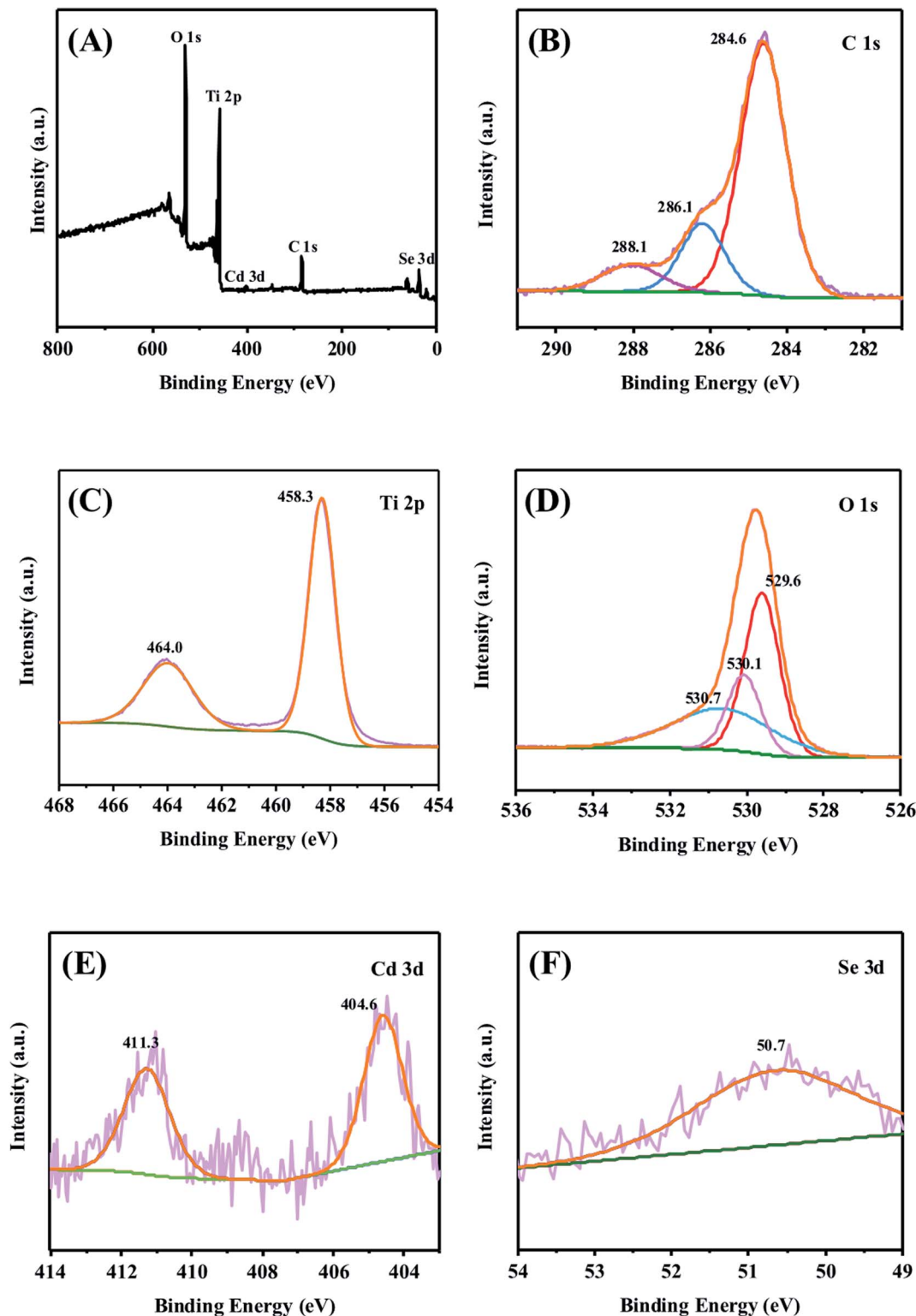
Fig. 4 (A) XPS survey spectrum of the CdSe/C/TiO$_2$ ternary nanofiber film, and high resolution spectra of (B) C 1s, (C) Ti 2p, (D) O 1s, (E) Cd 3d and (F) Se 3d.

highest V_{oc}, indicating that the charge separation efficiency is the best and more electrons can be accumulated. In addition, the linear sweep voltammetric curves (LSV) is recorded to determine the PEC property, as shown in Fig. 6C. CdSe/C/TiO$_2$

shows better PEC performance, achieving the highest current density than the others at an overpotential of 0.5 V. The synergistic effects of the carbon membrane and CdSe leads to
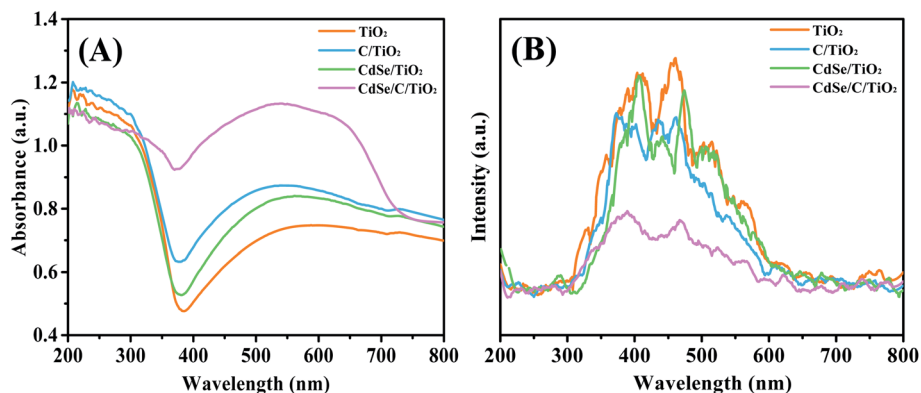
© 2021 The Author(s). Published by the Royal Society of Chemistry

Fig. 5 (A) UV-Vis diffuse reflectance spectra (DRS) of all samples and (B) PL spectra with the excitation wavelength of 220 nm.

an obvious enhancement of its PEC behavior. The result is consistent with the above photocurrent density and V_{oc} results.

To further understand the generation and accumulation properties of the carriers for all the samples, electrochemical impedance spectroscopy (EIS) was performed on different electrodes. The diameter of the semicircle in the Nyquist diagram expresses the resistance during charge transfer

processes.[62] Clearly, as shown in Fig. 6D, the resistance of TiO_2 is the largest, and the diameter of each composite is smaller than that of their single component. In particular, the diameter of $CdSe/C/TiO_2$ is the smallest, indicating that the electron transfer resistance is lowest and the charge transfer in the electrode is the fastest; therefore, the ternary composite possesses excellent PEC properties. In summary, the unique
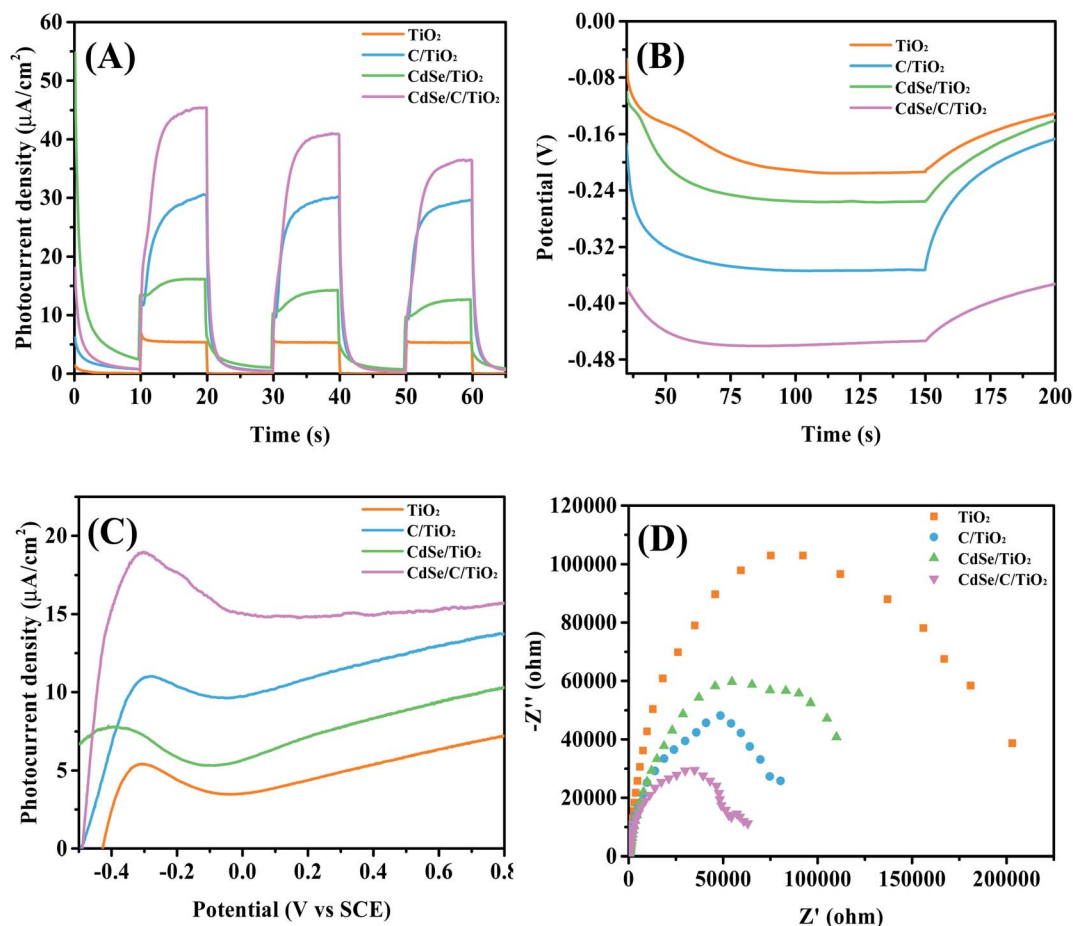

Fig. 6 (A) Transient photocurrent responses; (B) open circuit potential (*versus* SCE); (C) linear sweep voltammetry curves; (D) electrochemical impedance spectroscopy for pure TiO_2, C/TiO_2, $CdSe/TiO_2$ and $CdSe/C/TiO_2$ nanofilm.
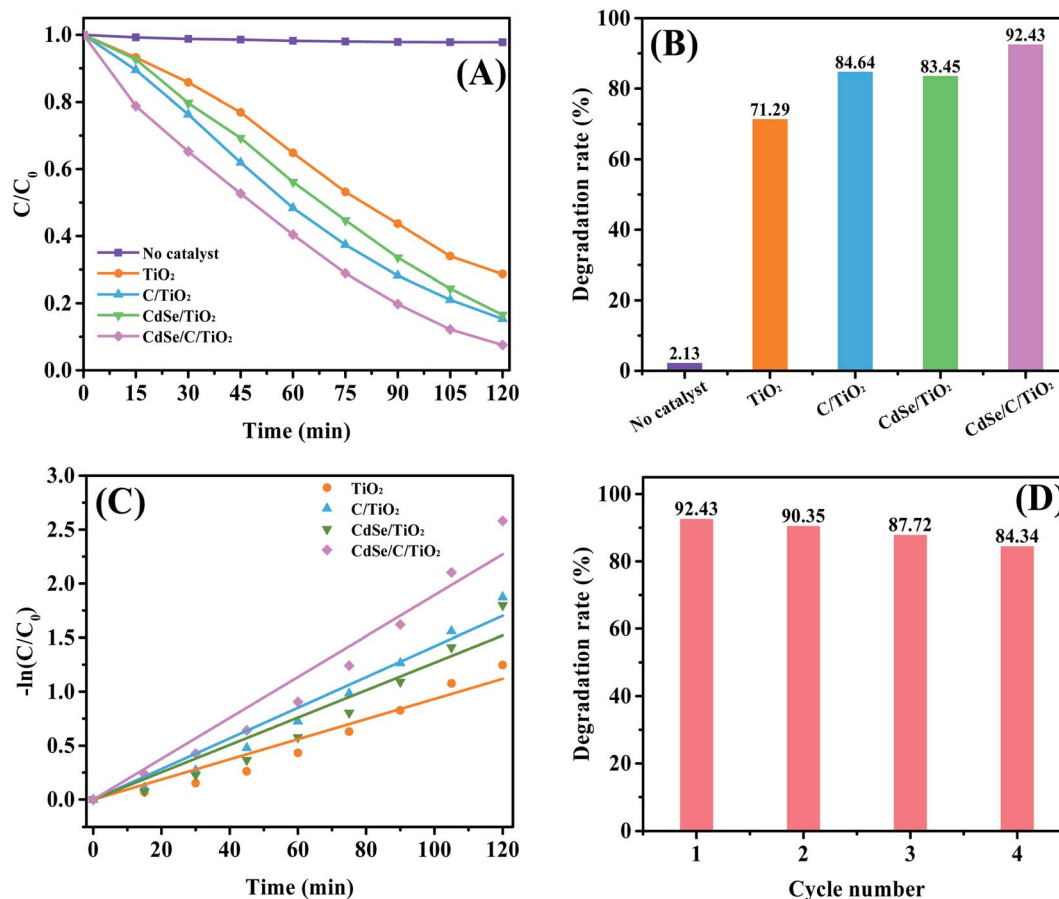
Fig. 7 (A) MB degradation by photoelectrocatalysis; (B) degradation rate of each samples at 120 min; (C) kinetics of MB degradation over pure TiO$_2$, C/TiO$_2$, CdSe/TiO$_2$ and CdSe/C/TiO$_2$; (D) reusability of the CdSe/C/TiO$_2$ nanofilm.
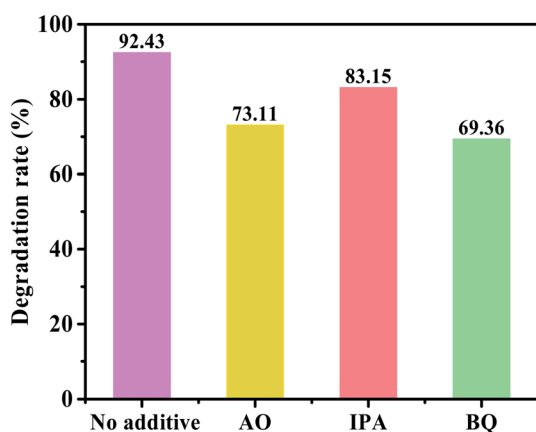

Fig. 8 The photoelectrocatalysis degradation of MB by CdSe/C/TiO$_2$ after the addition of h$^+$, ·OH and ·O$_2^-$ scavengers.

electron transfer property of the carbon membrane, as well as the synergistic effect with CdSe, can effectively inhibit the charge recombination and achieve higher PEC performance.

To further demonstrate the PEC property, the degradation efficiency of MB is illustrated in Fig. 7A and B, and the raw data for MB degradation is shown in Fig. S1.† Clearly, CdSe/C/TiO$_2$

can significantly achieve the removal of MB. Without the catalyst, only 2.13% of MB can be degraded after 120 min of light irradiation, indicating that MB can hardly induce self-degradation. Pure TiO$_2$ can only decompose 71.29% of MB, while the degradation efficiency of MB can reach 84.64%, 83.45% and 92.43% over C, CdSe, CdSe and C-modified samples, respectively. Therefore, the ternary CdSe/C/TiO$_2$ exhibits the best PEC activity with an improvement of 21.14% compared with pure TiO$_2$. In addition, the degradation kinetics of MB can be described as a pseudo-first-order reaction using the following formula:

$$\ln(C/C_0) = -kt \qquad (1)$$

where C_0 is the initial concentration of MB, C is the concentration of MB at given time t, and k is the kinetic rate constant.[63]

As shown in Fig. 7C, the kinetic rate constants for TiO$_2$, C/TiO$_2$, CdSe/TiO$_2$ and CdSe/C/TiO$_2$ electrode are approximately 9.33 × 10^{-3}, 14.18 × 10^{-3}, 12.67 × 10^{-3} and 18.93 × 10^{-3} min^{-1}, and marked as k_1, k_2, k_3 and k_4, respectively. The order of rate constants is $k_4 > k_2 > k_3 > k_1$, indicating that the CdSe/C/TiO$_2$ ternary composite has a faster degradation rate than the others. Furthermore, stability is also a key indicator of industrial applications of the catalyst. As shown in Fig. 7D,
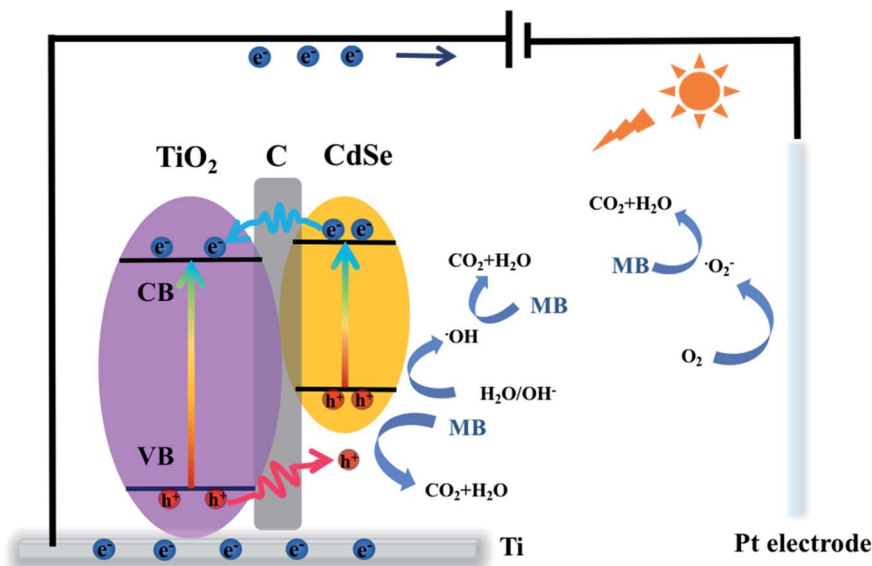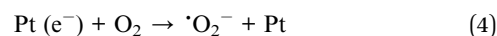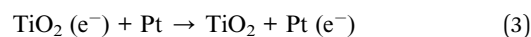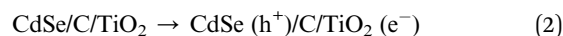
Fig. 9 The PEC mechanism of the MB degradation over the CdSe/C/TiO$_2$ nanofiber film.

when the catalyst is cycled four times, it is found that there is no significant decrease, indicating that the catalyst is stable.

Furthermore, PEC experiment was performed using different scavengers to reveal the role of the active substances. Here, 1,4-benzoquinone (BQ), ammonium oxalate (AO) and isopropanol (IPA) were used as the trapping agents for the superoxide radical scavenger ($\cdot O_2^-$), hole scavenger (h^+), and hydroxyl radical scavenger ($\cdot OH$), respectively.[64] Fig. 8 shows the results of the trapping experiment. It is clear that the degradation rate of CdSe/C/TiO$_2$ is 92.43% in the absence of the capture agent. When BQ and AO are added, the degradation rates decrease to 69.36% and 73.11%, respectively, indicating that $\cdot O_2^-$ and h^+ are the major active substances during the MB degradation. When IPA is added, the degradation rate is also affected, but the effects of $\cdot OH$ is relatively low.

According to the above-mentioned conclusions, a tentative mechanism is proposed to understand the degradation process. As shown in Fig. 9, electrons can be transferred from the valence band (VB) to the conduction band (CB) in TiO$_2$ and CdSe under light excitation. Holes from the VB of TiO$_2$ migrate to the VB of CdSe through the carbon membrane because of the potential difference, and then electrons transfer from the CB of CdSe to the CB of TiO$_2$ through the carbon membrane. Therefore, the carbon membrane plays a vital role as a carrier-transfer-channel between TiO$_2$ and CdSe. Subsequently, electrons will transport into the metal Ti through the TiO$_2$ nanofiber film, and continuously migrate to the Pt cathode under the bias potential. $\cdot O_2^-$ is generated from the reaction between the electron and the oxygen adsorbed on the surface of the cathode, and it can participate in the MB degradation process. Moreover, the carbon membrane can improve the interfacial contact between the semiconductor and the electrolyte, which promotes the contact between the holes and the organic pollutants during the degradation reaction, resulting in more h^+ to degrade MB.[65] This mechanism can be expressed by:

$$CdSe/C/TiO_2 \rightarrow CdSe\ (h^+)/C/TiO_2\ (e^-) \tag{2}$$

$$TiO_2\ (e^-) + Pt \rightarrow TiO_2 + Pt\ (e^-) \tag{3}$$

$$Pt\ (e^-) + O_2 \rightarrow \cdot O_2^- + Pt \tag{4}$$

$$h^+ + OH^-/H_2O \rightarrow \cdot OH \tag{5}$$

$$\cdot O_2^-/h^+/\cdot OH + MB \rightarrow CO_2 + H_2O \tag{6}$$

4. Conclusion

In summary, a CdSe/C/TiO$_2$ nanofiber film was developed for the photoelectrocatalytic degradation of MB. The CdSe/C/TiO$_2$ ternary composite exhibits a better PEC performance compared with its binary hybrids. The current density of the CdSe/C/TiO$_2$ nanofilm is about 9 times higher than that of pure TiO$_2$ under UV and visible light irradiations. V_{oc} and EIS results show that the CdSe/C/TiO$_2$ nanofiber film has better charge transfer capacity because the carbon membrane not only can greatly accelerate the carrier transfer as a carrier-transport-channel but can also improve the problem of the poor contact between the semiconductor and the electrolyte. The photoelectrocatalytic degradation of MB by CdSe/C/TiO$_2$ is significantly increased by about 21.14% than that of pure TiO$_2$. Therefore, the synergistic effects of the carbon membrane and CdSe endows the ternary composite sample CdSe/C/TiO$_2$ with excellent PEC performance. This study presents a great contribution to the preparation of highly efficient PEC degradation materials.

Author contributions

Xinye Zhang: writing, methodology, investigation, original draft. Xueyue Zhang: data curation, review & editing. Keting

Feng: formal analysis, review & editing. Xiaoyun Hu: supervision, review & editing. Jun Fan: review & editing. Enzhou Liu: project administration, funding acquisition.

Conflicts of interest

There are no conflicts to declare.

Acknowledgements

References

1 H. Zhou, Y. Qu, T. Zeid and X. Duan, *Energy Environ. Sci.*, 2012, **5**, 6732–6743.

2 C. Li, T. Lou, X. Yan, Y. Long, G. Cui and X. Wang, *Int. J. Biol. Macromol.*, 2018, **106**, 768–774.

3 T. Robinson, G. McMullan, R. Marchant and P. Nigam, *Bioresour. Technol.*, 2001, **77**, 247–255.

4 U. Habiba, T. A. Siddique, T. C. Joo, A. Salleh, B. C. Ang and A. M. Afifi, *Carbohydr. Polym.*, 2017, **157**, 1568–1576.

5 H. She, H. Zhou, L. Li, L. Wang, J. Huang and Q. Wang, *ACS Sustainable Chem. Eng.*, 2018, **6**, 11939–11948.

6 M. Zhou, Q. Dai, L. Lei, C. Ma and D. Wang, *Environ. Sci. Technol.*, 2005, **39**, 363–370.

7 W. Przystaś, E. Zabłocka-Godlewska and E. Grabińska-Sota, *Water, Air, Soil Pollut.*, 2012, **223**, 1581–1592.

8 A. Xu, W. Tu, S. Shen, Z. Lin, N. Gao and W. Zhong, *Appl. Surf. Sci.*, 2020, **528**, 146949.

9 H. Dong, X. Guan, D. Wang, C. Li, X. Yang and X. Dou, *Chemosphere*, 2011, **85**, 1115–1121.

10 I. Oller, S. Malato and J. A. Sánchez-Pérez, *Sci. Total Environ.*, 2011, **409**, 4141–4166.

11 Y. Zhou, L. Tang, G. Zeng, J. Chen, Y. Cai, Y. Zhang, G. Yang, Y. Liu, C. Zhang and W. Tang, *Biosens. Bioelectron.*, 2014, **61**, 519–525.

12 W. Zhong, Z. Wang, N. Gao, L. Huang, Z. Lin, Y. Liu, F. Meng, J. Deng, S. Jin, Q. Zhang and L. Gu, *Angew. Chem., Int. Ed.*, 2020, **59**, 22743–22748.

13 M. A. Ahmed, M. F. Abdel-Messih and E. H. Ismail, *J. Mater. Sci.: Mater. Electron.*, 2019, **30**, 17527–17539.

14 D. Cao, Y. Wang, M. Qiao and X. Zhao, *J. Catal.*, 2018, **360**, 240–249.

15 K. Wang, Y. Zhang, L. Liu, N. Lu and Z. Zhang, *J. Mater. Sci.*, 2019, **54**, 8426–8435.

16 M. Shaban, A. M. Ahmed, N. Shehata, M. A. Betiha and A. M. Rabie, *J. Colloid Interface Sci.*, 2019, **555**, 31–41.

17 Z. Wang, Z. Lin, J. Deng, S. Shen, F. Meng, J. Zhang, Q. Zhang, W. Zhong and L. Gu, *Adv. Energy Mater.*, 2021, **11**, 2003023.

18 M. Li, H. Liu, Y. Song and J. Gao, *Int. J. Energy Res.*, 2018, **42**, 4625–4641.

19 Z. Zeng, F. Xiao, X. Gui, R. Wang, B. Liu and T. T. Y. Tan, *J. Mater. Chem. A*, 2016, **4**, 16383–16393.

20 Q. Ma, H. Wang, H. Zhang, X. Cheng, M. Xie and Q. Cheng, *Sep. Purif. Technol.*, 2017, **189**, 193–203.

21 A. Fujishima and K. Honda, *Nature*, 1972, **238**, 37–38.

22 S. U. M. Khan, M. Al-Shahry and W. B. Ingler Jr, *Science*, 2002, **297**, 2243–2245.

23 Y. Yang, L. C. Kao, Y. Liu, K. Sun, H. Yu and J. Guo, *ACS Catal.*, 2018, **8**, 4278–4288.

24 W. Ouyang, F. Teng and X. Fang, *Adv. Funct. Mater.*, 2018, **28**, 1707178–1707190.

25 J. Xue, O. Elbanna, S. Kim, M. Fujitsuka and T. Majima, *Chem. Commun.*, 2018, **54**, 6052–6055.

26 K. He, Z. Zeng, A. Chen, G. Zeng, R. Xiao, P. Xu, Z. Huang, J. Shi, L. Hu and G. Chen, *Small*, 2018, **15**, 1800871.

27 W. T. Chen, A. Chan, D. X. S. Waterhouse, J. Llorca, H. Idriss and G. I. N. Waterhouse, *J. Catal.*, 2018, **367**, 27–42.

28 J. Yi, S. Zhang, H. Wang, H. Yu and F. Peng, *Mater. Res. Bull.*, 2014, **60**, 130–136.

29 Y. Zhu, Y. Wang, Z. Chen, L. Qin, L. Yang, L. Zhu, P. Tang, T. Gao, Y. Huang, Z. Sha and G. Tang, *Appl. Catal., A*, 2015, **498**, 159–166.

30 G. Li, D. Zhang and J. Yu, *Environ. Sci. Technol.*, 2009, **43**, 7079–7085.

31 T. ThanhThuy, H. Feng and Q. Cai, *Chem. Eng. J.*, 2013, **223**, 379–387.

32 J. Jia, P. Xue, X. Hu, Y. Wang, E. Liu and J. Fan, *J. Catal.*, 2019, **375**, 81–94.

33 W. Zhong, B. Xiao, Z. Lin, Z. Wang, L. Huang, S. Shen, Q. Zhang and L. Gu, *Adv. Mater.*, 2021, **33**, 202007894.

34 J. Pan, Y. Sheng, J. Zhang, J. Wei, P. Huang, X. Zhang and B. Feng, *J. Mater. Chem. A*, 2014, **2**, 18082–18086.

35 M. Y. A. Rahman, S. N. Sadikin and A. A. Umar, *Appl. Phys. A*, 2018, **124**, 460.

36 F. Xiao, J. Miao, H. Wang, H. Yang, J. Chen and B. Liu, *Nanoscale*, 2014, **6**, 6727–6737.

37 V. Nguyen, W. Li, V. Pham, L. Wang, P. Sheng, Q. Cai and C. Grimes, *J. Colloid Interface Sci.*, 2016, **462**, 389–396.

38 H. Li, X. Wang, L. Zhang and B. Hou, *Corros. Sci.*, 2015, **94**, 342–349.

39 Y. Song, N. Li, D. Chen, Q. Xu, H. Li, J. He and J. Lu, *ACS Sustainable Chem. Eng.*, 2018, **6**, 4000–4007.

40 Y. Chang, P. Hsieh, T. M. Chang, C. Chen, M. Sone and Y. Hsu, *J. Mater. Chem. A*, 2020, **8**, 13971–13979.

41 P. Xue, Y. Yin, Y. Wang, J. Wan, Y. Ma, E. Liu, X. Hu and J. Fan, *Semicond. Sci. Technol.*, 2017, **32**, 115007.

42 D. Xu, B. Liu, W. Zou, H. Wang and C. Zhang, *Appl. Surf. Sci.*, 2019, **487**, 91–100.

43 T. Ju, H. Lee and M. Kang, *J. Ind. Eng. Chem.*, 2014, **20**, 2636–2640.

44 Y. Cong, X. Lia, Y. Qin, Z. Dong, G. Yuan, Z. Cui and X. Lai, *Appl. Catal., B*, 2011, **107**, 128–134.

45 G. S. Selopal, M. Mohammadnezhad, L. V. Besteiro, O. Cavuslar, J. Liu, H. Zhang, F. Navarro-Pardo, G. Liu, M. Wang, E. G. Durmusoglu, H. Y. Acar, S. Sun, H. Zhao, Z. M. Wang and F. Rosei, *Adv. Sci.*, 2020, **7**, 2001864.

46 Y. Li, C. Chen, M. Wang, W. Li, Y. Wang, L. Jiao and H. Yuan, *J. Power Sources*, 2017, **361**, 326–333.

47 X. Zhang, H. Huang, J. Liu, Y. Liu and Z. Kang, *J. Mater. Chem. A*, 2013, **1**, 11529–11533.

48 X. Zhang, P. Xue, J. Jia, X. Hu, J. Fan and E. Liu, *Nanotechnology*, 2019, **30**, 435403.

49 G. Xie, K. Zhang, B. Guo, Q. Liu, L. Fang and J. Gong, *Adv. Mater.*, 2013, **25**, 3820–3839.

50 L. Tan, N. Li, S. Chen and Z. Liu, *J. Mater. Chem. A*, 2016, **4**, 12273–12280.

51 B. Gao, M. Sun, W. Ding, Z. Ding and W. Liu, *Appl. Catal., B*, 2021, **281**, 119492.

52 E. Liu, C. Xu, C. Jin, J. Fan and X. Hu, *J. Taiwan Inst. Chem. Eng.*, 2019, **97**, 316–325.

53 E. Liu, X. Zhang, P. Xue, J. Fan and X. Hu, *Int. J. Hydrogen Energy*, 2020, **45**, 9635–9647.

54 W. Wang, F. Li, D. Zhang, D. Leungb and G. Li, *Appl. Surf. Sci.*, 2016, **362**, 490–497.

55 Y. Cong, X. Li, Y. Qin, Z. Dong, G. Yuan, Z. Cui and X. La, *Appl. Catal., B*, 2011, **107**, 128–134.

56 Y. Lin, C. Lin, J. Miller, Y. Hsu, Y. Chen, L. Chen and K. Chen, *RSC Adv.*, 2012, **2**, 11258–11262.

57 H. Yu, Y. Zhao, C. Zhou, L. Shang, Y. Peng, Y. Cao, L. Wu, C. Tung and T. Zhang, *J. Mater. Chem. A*, 2014, **2**, 3344–3351.

58 J. Pan, Y. Sheng, J. Zhang, J. Wei, P. Huang, X. Zhang and B. Feng, *J. Mater. Chem.*, 2014, **2**, 18082–18086.

59 Y. Liang, B. Kong, A. W. Zhu, Z. Wang and Y. Tian, *Chem. Commun.*, 2012, **48**, 245–247.

60 Z. Zhang, B. Chen, H. Xu, Z. Cui, S. Dong, A. Du, J. Ma, Q. Wang, X. Zhou and G. Cui, *Adv. Funct. Mater.*, 2018, **1**, 1701718.

61 D. Zhang, X. Yang, J. Zhu, Y. Zhang, P. Zhang and G. Li, *J. Sol-Gel Sci. Technol.*, 2011, **58**, 594–601.

62 Q. Wang, J. Huang, H. Sun, K. Zhang and Y. Lai, *Nanoscale*, 2017, **9**, 16046–16058.

63 H. A. Hamad, W. A. Sadik, M. M. El-latif, A. B. Kashyout and M. Y. Feteha, *J. Environ. Sci.*, 2016, **43**, 26–39.

64 D. Liu, R. Tian, J. Wang, E. Nie, X. Piao, X. Li and Z. Sun, *Chemosphere*, 2017, **185**, 574–581.

65 Z. Liu, J. Zhang and W. Yan, *ACS Sustainable Chem. Eng.*, 2018, **6**, 3565–3574.